International Journal of Biological Macromolecules 130 (2019) 1009–1017

Contents lists available at ScienceDirect

International Journal of Biological Macromolecules

journal homepage: http://www.elsevier.com/locate/ijbiomac

Stimuli-responsive injectable cellulose thixogel for cell encapsulation

Naresh D. Sanandiya [a], Jyothsna Vasudevan [a,b], Rupambika Das [a], Chwee Teck Lim [b,c,d], Javier G. Fernandez [a,*]

[a] Singapore University of Technology & Design, 8 Somapah Road, Singapore 487372, Singapore
[b] Department of Biomedical Engineering, National University of Singapore, Singapore 117583, Singapore
[c] Biomedical Institute for Global Health Research and Technology, National University of Singapore, MD6, 14 Medical Drive, #14-01, Singapore 117599, Singapore
[d] Mechanobiology Institute, National University of Singapore, Singapore 117411, Singapore

ARTICLE INFO

Article history:
Received 25 January 2019
Received in revised form 22 February 2019
Accepted 22 February 2019
Available online 06 March 2019

Keywords:
Cellulose
Thixotropy
Injectable hydrogel

ABSTRACT

Herein, we present the synthesis of surface-oxidized cellulose nanofiber (CNF) hydrogel and characterization with various physicochemical analyses and spectroscopic tools as well as its suitability for cellular encapsulation and delivery. The structure-property relationship as shear thinning, thixotropy, creep-recovery and stimuli responsiveness are explored. The CNF hydrogel is capable to inject possessing shear thinning behavior at shear rate (~10 s^{-1}) range in the normal injecting process. In time-dependent thixotropy, the hydrogel showed rapid transform from flowable fluid back to structured hydrogel fully recovering in less than 60 s. The presence of cell-culture media did not alter shear thinning behavior of CNF hydrogel and showed increased thixotropicity with respect to the control gel. The CNF hydrogel forms 3D structures, without any crosslinker, with a wide range of tunable moduli (~36–1000 Pa) based on concentration and external stimuli. The biological characteristics of the thixotropic gels are studied for human breast cancer cells and mouse embryonic stem cells and indicated high cell viability, long-term survival, and spherical morphology.

1. Introduction

Polymeric hydrogels are at the forefront of cell-encapsulation and delivery technologies. They are highly hydrated molecular networks, with characteristics similar to those of an extracellular matrix, that enable fluent diffusion of biomolecules [1]. Based on their functions, there are two main types of hydrogels currently in use in tissue engineering: those forming cell-laden mechanically robust structures *in vitro* that are later implanted, and those hydrogels with fluid characteristics that can be sprayed or injected [2–4]. These mutually exclusive characteristics limit the general utility of most hydrogels for various applications. Solid hydrogels provide a good protective environment and encapsulation for the new cells but can result in trauma from surgical implantation. Additionally, solid hydrogels lack the ability to adapt to the geometry and mechanical properties of the host tissue, which is required to establish an optimal host-implant interaction [5]. On the other hand, most injectable hydrogels fail to retain structural integrity after injection, offering a limited ability to retain the encapsulated cells [6].

A wide variety of hydrogels, of both natural and synthetic origin, such as polycaprolactone [7], poly(ethylene glycol) [8], sodium alginate [9,10], pectin [11], and gelatin [12], have been reported for cell-delivery applications. However, their hydrogel structures lack mechanical robustness or multifaceted systems, or they require chemical modification, irradiation, or a secondary crosslinking component for advanced applications [13–16].

By contrast, cellulose nanofibers (CNF) is a form of nanocellulose material with a high aspect ratio (10–50 nm wide, 500–2000 nm long) and an anionic charge on the surface. It forms robust hydrogels without any additives at low concentrations by anion–anion repulsion, in addition to their hydrogen-bonding nature. [17,18]. Chemically, CNF is similar to the glucuronate-block of the alginate which is widely used in tissue engineering. Despite this, the alginate shows feeble thixotropicity and recovery limiting it to form a confined structure [16,19]. Furthermore, at low concentrations and at shear rates >10 s^{-1}, unmodified alginate shows Newtonian characteristics which is not suitable in injectable systems [20,21]. CNF forms 3D networks of entangled flexible nanofibers linked *via* water-mediated hydrogen bonds, leading to the formation of hydrogels with a confined structure [22]. Several studies have been conducted to fabricate CNF hydrogels for application in various domains; however, to the best of our knowledge, the detailed flow behavior, structure–property relationship, and effect of cell-culture media on CNF hydrogels have not yet been explored for cell-encapsulation applications.

We present here a multi-stimulus responsive cellulose thixogel for potential applications in tissue engineering. Its transition between injectable and solid forms, as well as its ability to encapsulate and deliver cells, were investigated. Key requirements for the developed cell carrier were (i) the hydrogel matrix must be preloaded with cells, promoting even distribution after transplantation and long-term survival using a

* Corresponding author.
E-mail address: javier.fernandez@sutd.edu.sg (J.G. Fernandez).

https://doi.org/10.1016/j.ijbiomac.2019.02.135
0141-8130/

minimally-invasive technique, such as injection; (ii) the hydrogel must show shear-thinning characteristics to mitigate the effect of shear forces on cells during injection, improving the survival and outcome of cell-based therapies; (iii) the hydrogel should show thixotropic behavior, enabling the rapid transformation of the hydrogel to a robust and protective encapsulation after injection; and (iv) the transition between a fluid and solid hydrogel should ideally be triggered not only by the injection process, but also by other mechanical (*e.g.* sonication, stirring, or shaking) or chemical means. Additionally, having both reversible and irreversible processes would broaden the applicability of the hydrogel to technologies requiring fast and stable encapsulation, such as 3D bioprinting.

2. Materials and methods

2.1. Materials

2,2,6,6-Tetramethylpiperidine 1-oxyl (TEMPO), sodium bromide (NaBr; ≥99%), sodium hypochlorite (NaClO; 5% available chlorine), sodium hydroxide (NaOH; ≥99%), and hydrochloric acid (HCl; 37%) of analytical reagent (AR) grade were used, all purchased from Sigma-Aldrich Pte Ltd., Singapore. All reagents, unless otherwise specified, were used as received, without further purification. Filter paper, made from 100% virgin pulp, from local suppliers was used as a cellulose source. Dulbecco's modified Eagle's medium (DMEM), phosphate buffered saline (1×) (PBS), and 10,000 U/ml penicillin-streptomycin mixed solution were purchased from Nacalai Tesque, Kyoto, Japan. Fetal bovine serum (FBS) was purchased from Gibco (ThermoFisher, USA). MCF-7, E14TG2A (ATCC, USA), calcein-AM/ethidium homodimer-1 viability/cytotoxicity kits (LIVE/DEAD®, Invitrogen, ThermoFisher Scientific, USA), 24-well plates (CELLSTAR®, Sigma-Aldrich, Singapore), elastomer, and curing agent for polydimethylsiloxane (PDMS) molds (SYLGARD® 184, Sigma-Aldrich, Singapore) were all used as received.

2.2. Synthesis of CNF hydrogel

CNF preparation was carried out by TEMPO-mediated oxidation of filter-paper cellulose, using a previously reported method with minor modifications (Fig. 1A) [17,23]. Briefly, the cellulose (2 g, 12 mmol anhydroglucose units; AGU) was submerged in deionized (DI) water (200 ml) containing TEMPO (31.2 mg, 0.2 mmol) and NaBr (205 mg, 2 mmol) under stirring at 25 °C. The NaOCl solution (5% w/v, 27 ml, 20 mmol) was added drop-wise and the pH was maintained at 10.5 by adding 0.5 M NaOH solution until no more variation was observed. The oxidized cellulose material was rinsed several times with DI water until the final pH reached 7.4, followed by homogenization using an ultrasonic probe homogenizer (Fisherbrand™ Model 505) at 1% (w/v) concentration. The prepared hydrogel was stored at 4 °C before further use or analysis.

2.3. Characterization of CNF

Fourier transform infrared (FTIR) spectra of cellulose and dried CNF were obtained using an FTIR spectrometer (VERTEX 70 FTIR, Bruker Optik GmbH, Germany) with a resolution of 4 cm^{-1} and accumulation of 32 scans between 4000 and 400 cm^{-1} on ATR mode. The FTIR spectra of CNF were recorded in the acidic conditions used for transforming carboxylate to the carboxylic functional group, to avoid resonance overlapping with hydroxyl groups [24]. The surface morphology and nanostructures of the cellulose and CNF were examined using a field emission scanning electron microscope (FESEM; JSM-7600F, JEOL, Japan) at 5 kV accelerating voltage. Freeze-dried samples were mounted onto a carbon tape on an aluminum stub and sputter coated with gold for 30 s. X-ray diffraction (XRD) patterns of cellulose and CNF were obtained using an XRD system (D8 Discover, Bruker, USA), using nickel-filtered Cu-Kα radiation (λ = 0.15418 nm) operated at 40 mA and 40 kV, with a scan speed of 3°min^{-1}, having set the 2θ angle from 2° to 45°. The crystallinity indices (CI) were calculated using the Segal Method by the following equation (Eq. (1)) [25]:

$$CI = \frac{(I_{002} - I_{am})}{I_{002}} \times 100 \quad (1)$$

where I_{002} is the maximum intensity of 002 lattice diffraction, and I_{am} is the intensity of the amorphous region at $2(\theta) = 18°$.

2.4. Degree of oxidation

The degree of oxidation (D_O) of the obtained CNF hydrogel was estimated by conductivity titration [26], which refers to the average number of carboxylic groups per anhydroglucose unit. CNF hydrogel (~0.3 g corresponding dry weight) was dispersed in 50 mL of water, and 0.05 M HCl solution was added drop-wise, with stirring, to reach pH 2.5, followed by conductivity titration with 0.05 M NaOH solution at an addition rate of 0.1 ml min^{-1} at 25 °C. The degree of oxidation was calculated using the following equation (Eq. (2)):

$$D_O = \frac{162\,(V_2 - V_1)c}{w - 36(V_2 - V_1)c} \quad (2)$$

where V_1 is the volume of NaOH required to achieve neutralization of the strong acid (HCl), V_2 is the volume of NaOH required for neutralization of the weak acid (—COOH), c is the concentration of NaOH (mol l^{-1}), and w is the dry amount of the cellulose nanofibers.

2.5. Rheological characteristics

The CNF hydrogel of 1% concentration was further diluted separately to 0.75% and 0.5% w/w concentrations with DI water, as well as with media for conducting rheological experiments. All the rheological experiments with the CNF hydrogel were performed using a rheometer (HR-2 Discovery Hybrid Rheometer equipped with Environmental Test Chamber, TA Instruments, USA), using parallel plate geometry (40 mm diameter, 1 mm gap). The temperature was maintained at 25 °C by active temperature control (ACT) and a circulating water bath. The flow behaviors of the CNF hydrogels of different concentrations were determined by measuring the dynamic shear viscosity (η) with different shear rates (0.01–1000 s^{-1}). A power law model was fitted to the plot, representing shear stress as a function of shear rate (Eq. (3)):

$$\tau = K\dot{\gamma}^{n} \quad (3)$$

Here, K is the consistency coefficient and n is the flow behavior index; τ and $\dot{\gamma}$ represent the shear stress and applied shear rate, respectively. The Casson fluid model was also fitted to the plot representing shear stress as a function of shear rate using TRIOS software (TA Instruments, USA). Experiments for evaluating the time-dependent thixotropic property of CNF were carried out at different three-step shear rates (0.1 s^{-1}, 100 s^{-1}, and 0.1 s^{-1}), employing durations of 100 s for each step [15,19]. The total thixotropy times of the hydrogel samples were determined by the time differences between the second step at the end of the structural deformation phase and the time during the third stage when the maximum viscosity was achieved as a result of structural regeneration. The thixotropy of the hydrogel was measured with a hysteresis loop method in which the shear rates applied were varied from 0.1 to 1000 s^{-1} for 300 s in an upward sweep, immediately followed up by a downward sweep. Areas under the upstream (A_{up}) and the downstream (A_{down}) data points, as well as the hysteresis (thixotropic) area ($A_{up} - A_{down}$), were obtained using the TRIOS

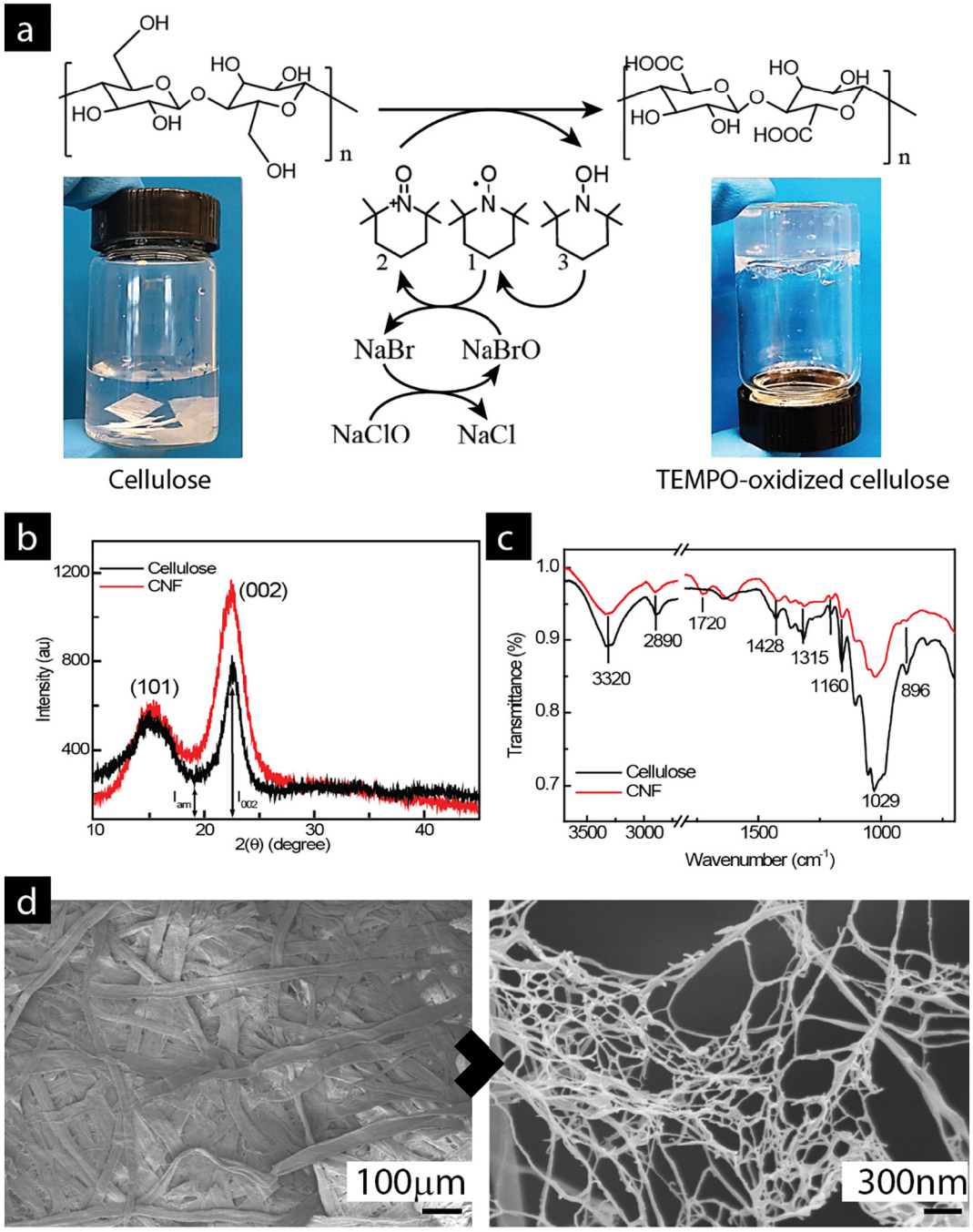

Fig. 1. Synthesis and characterization of CNF. (a) Reaction mechanism of the TEMPO-mediated surface oxidation of primary hydroxyls of cellulose followed by mechanical disintegration, leading from cellulose paper to transparent hydrogel. (b) X-ray diffractograms of cellulose and CNF. (c) FTIR spectra of cellulose and CNF. (d) Scanning electron micrographs of cellulose and CNF.

software. The percentage of relative thixotropic area (A_r) was calculated using Eq. (4) [27]:

$$A_r = \frac{(A_{up} - A_{down})}{(A_{up})} \times 100 \quad (4)$$

An oscillation-strain sweep, from 0.001 to 100% strain at an angular frequency of 10 rad s^{-1}, was performed to detect the linear viscoelastic region (LVR). Further, an oscillation frequency sweep in these LVRs was performed in a range of 0.1–100 rad s^{-1} to measure the storage and loss moduli. The time-relaxation thixotropy of the CNF hydrogel was carried out by measuring storage (G′) and loss moduli (G″) at strain in the LVR (strain 1%) for 150 s at 1 Hz frequency followed by deformation of the gel employing strain greater than LVR (strain 20%) for 60s at 1 Hz frequency [28]. The cycle was further repeated five times. The yield stress (τ) experiment for each sample was carried out at a constant shear rate as a function of time. The static yield stress for each sample was ascertained, which represents the range of linear reversible deformation for a soft gel system. For the creep-recovery measurement, all samples were subjected to an applied creep for 300 s, while the recovery was observed for 600 s.

2.6. Water holding capacity of CNF hydrogel

The CNF hydrogel was dispersed in cell-culture media (7:3 ratio of water to media), and the final concentration was set to 0.5% (w/w).

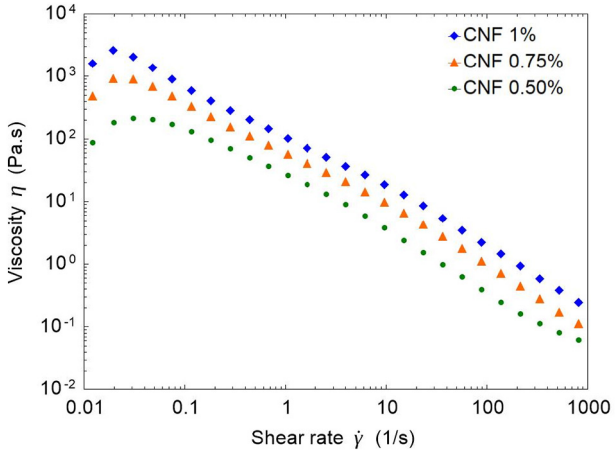

Fig. 2. Shear-thinning behavior of the CNF hydrogel by dynamic viscosity curves.

The prepared hydrogel (3 g) was placed in a petri dish containing a buffer solution of different pH values (4.0, 7.4, and 9.0) and incubated at 37 °C for 48 h. The water holding capacity Q (g/g) of the hydrogel was calculated at predetermined interval of time from the following expression (Eq. (5)):

$$Q = \frac{(W_1 - W_0)}{(W_0)} \tag{5}$$

Here, W_0 is the initial weight of the hydrogel, and W_1 is the final weight of the hydrogel.

2.7. 3D cell culture and encapsulation

Two separate cell lines, green fluorescent protein (GFP) expressing human breast cancer (MCF-7) and mouse embryonic stem cells (mESC; E14TG2A), were used to perform the encapsulation and viability assays. The MCF-7 cell line was cultured in DMEM supplemented with 10% (v/v) FBS and 1% (v/v) penicillin-streptomycin mixed solution and maintained at 37 °C in a humidified atmosphere with 5% CO_2. E14TG2A mESCs were grown on a 0.1% (w/v) gelatinized petri dish containing DMEM supplemented with 1% v/v sodium pyruvate, 1% (v/v) L-glutamine, 1× (v/v) non-essential amino acids, 15% (v/v) FBS, 1% (v/v) penicillin-streptomycin, 0.1 mM (v/v) 2-mercaptoethanol, and leukemia inhibiting factor (LIF; 1000 U/ml).

Upon confluency, the MCF-7 cells were dissociated using trypsin, centrifuged, and re-suspended in fresh medium at a concentration of 9×10^5 cells/ml. The cells were encapsulated in CNF hydrogel under sterile conditions. The hydrogel was initially vortexed at high speed for 5 min to lower the viscosity. This solution was mixed homogeneously with the cell suspension and then seeded into 24-well plates. The hydrogel was incubated in medium and maintained at 37 °C, 5% CO_2. The culture medium was replaced every 24 h. All samples were prepared in triplicate. A LIVE/DEAD® viability/cytotoxicity assay kit was used to test the viability of the encapsulated cells. The reagents were added to the hydrogel, followed by incubation for 45 min in the dark at 37 °C. Green (live cells) and red (dead cells) fluorescence images, along with corresponding phase contrast images, were collected separately using an inverted microscope (Axio Observer, Carl Zeiss GmbH, Germany). Similarly, 1×10^6 mESCs were added to the cellulose hydrogel contained in a 24-well plate at a 1:1 ratio. The cells were pipetted thoroughly to uniformly disperse them in the gel. After 24 h, the plate was incubated for 45 min in the dark using a LIVE/DEAD® viability/cytotoxicity kit, and representative images were taken. Viability was checked periodically at 1, 3, 5 and 7 days.

To obtain a 3D overview of the cell-laden hydrogel constructs using confocal microscopy, a mold was designed using a solid-modeling computer aided design (CAD) computer program (SolidWorks, Dassault Systèmes, France). 3D printing of the mold was achieved using a high-precision 3D printer (Objet30 Prime, Stratasys, USA). The molds were washed thoroughly with distilled water and dried at 60 °C prior to use. A PDMS replica was molded by casting a liquid pre-polymer

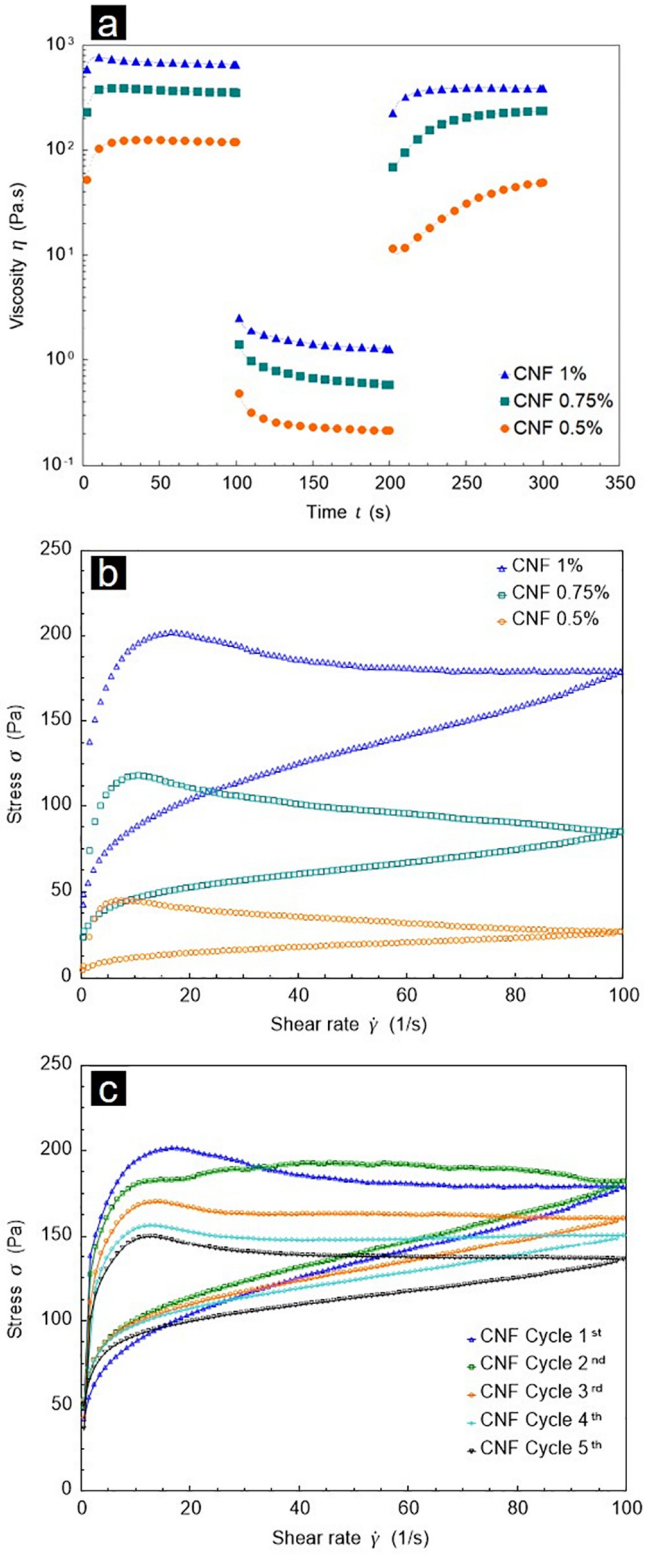

Fig. 3. Thixotropic behavior of CNF hydrogel. (a) Time-dependent thixotropicity behavior of the CNF hydrogel by step shear measurements. (b) Evaluation of the thixotropicity by a hysteresis loop test of CNF hydrogel at 1, 0.75, and 0.5% concentrations. (c) Recovery of thixotropicity by a cycle performance test for five consecutive cycles.

Table 1
Deformation and recovery characteristics of CNF hydrogels.

Entry	CNF concentration, (%)	Yield stress, τ_0 (Pa)	Maximum creep, γ (%)	Relative recovery, R (%)
1	1	55.88	33.14	18.94
2	0.75	23.08	42.87	25.84
3	0.50	6.89	190.81	69.13

comprising a mixture of 10:1 elastomer and curing agent. The mixture was cured at 60 °C overnight and the PDMS mold was peeled off the 3D-printed mold. The PDMS mold was plasma bonded (Harrick Plasma, USA) to a coverslip (22 × 22 mm) for 5 min. 200 μl of cell-laden hydrogel was injected into the center, and close contact with a coverslip was ensured. The gel construct was immersed in culture media and the media was replenished every 24 h. After 96 h of cultivation, the constructs were visualized using a confocal laser scanning microscope (AR1, Nikon Corp, Japan). The hydrogel construct was excited at 488 nm and Z-stack images were taken through a hydrogel depth of 600 μm with an interval of 10 μm between each image.

3. Results and discussion

3.1. Synthesis and characterization of stimuli-responsive cellulose hydrogel

To prepare the cellulose-based hydrogel, regioselective surface oxidation of the primary hydroxyl groups of the cellulose was conducted using a TEMPO radical-mediated system, as shown in Fig. 1a. The oxidized cellulose was further disintegrated using a probe sonicator, leading to the formation of the CNF hydrogel in water with 26% oxidation (Fig. S1). XRD and FTIR were used to characterize the cellulose oxidation (Fig. 1b & c). The integrity of the cellulose backbone was confirmed by the presence of its characteristic IR bands. The oxidation of the CNF was confirmed with a noticeable new sharp peak at 1720 cm^{-1}, attributed to the vibration mode of —C═O in the carboxylic acid. The absence of prominent IR bands in the CNF sample at 2971, 1460, and 1238 cm^{-1} attributable to the methyl, aromatic methylene, and —N—O resonance of the TEMPO reagents confirmed the complete removal of the oxidizing reagent (Fig. S2). Despite the oxidation of the cellulose, the crystallinity remained intact (Fig. 1b), showing the characteristic cellulose I diffraction pattern with peaks at 15° (101) and 22° (002) [29]. Unmodified cellulose exhibited a micro-fibrous structural morphology of several millimeters, with widths in the range of 30–70 μm (Fig. 1d). However, the oxidized cellulose was characterized by a highly entangled and inherently joint fibrils network, with diameters in the range of 40–100 nm.

3.2. Shear-thinning behavior of the hydrogel

Shear-thinning hydrogels can flow and deform into liquids under shear stress due to the alignment of polymeric chains/fibers in flow direction and loss of chain entanglements (Fig. S3; Movie S1). In biomedical applications, these hydrogels can be cell-laden, are able to absorb shear forces, and can prevent cellular damage during injection, thus

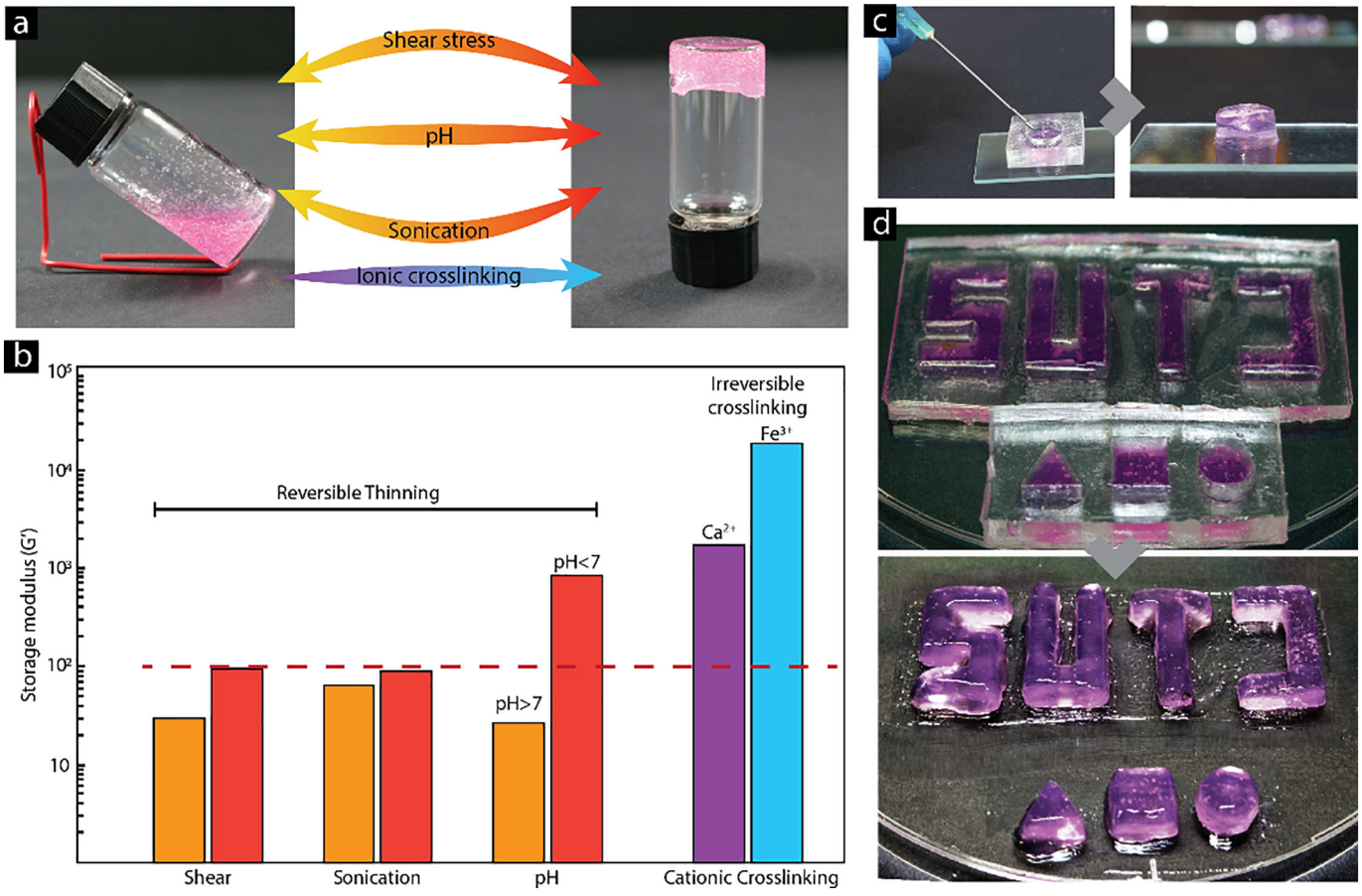

Fig. 4. Characterization of CNF thixotropy. (a) Stimulus responsiveness of CNF hydrogel for stress, sonication, pH, and cation factors (white spots in the hydrogel are micro-bubbles formed by cavitation during vortex agitation). (b) Range of storage modulus (G′) obtained with various stimulus factors. (c) Injection of CNF hydrogel in a cylindrical mold. The hydrogel was injected in a low-viscosity state, enabling its delivery, but rapidly recovered its consistency after being deposited, retaining the shape of the mold. (d) Additional examples of shape conformation after injection. The hydrogel conformed to complex structures and narrow spaces before returning to its solid state.

mitigating the effects of shear forces on cells and thereby improving the outcomes of cell-based therapeutics [30]. The dynamic viscosities (η) of CNF hydrogels with different water amounts were examined as a function of shear rate (Fig. 2; Table S1). The higher polymer/water ratio exhibited greater viscosity along the entire range of the shear rate, indicating a more entangled polymeric network. Furthermore, while the range of viscosities achievable by the hydrogel was strongly influenced by its water content, all hydrogels showed a decrease in viscosity under shear. The flow behavior index was $n < 1$, as derived from the power law approximation curve, indicating the typical shear-thinning behavior of the samples. The standard flow curves were fitted to different fluid models; the best fit of the statistical data (maximum R^2 value) to the Casson fluid model indicates a non-Newtonian fluid with yield stress (Table S2) [31]. The CNF hydrogels exhibited low viscous behavior at moderate shear rates (~10 s^{-1}), such as those produced during an injection process [32]. A plateau region was observed at high shear rates (>10 s^{-1}), suggesting homogeneity in the aspect ratio of the nanofibrils [33].

Due to the medical nature of the technology, the shear-thinning characteristics of the material were also studied after changing the dispersal phase of the CNF hydrogels from water to DMEM, enabling the support of cellular metabolism after encapsulation. While the shear-thinning characteristics of the hydrogel were unaffected by the change, the presence of media produced some distinctive differences in the flow curve, specifically, higher viscosities at lower shear rates (γ• > 1 s^{-1}) than the respective water-based sample, suggesting a new interaction of the CNF polymer with, probably, the sucrose present in the media (Fig. S4) [34].

3.3. Structural deformation and regeneration of the hydrogel

Structural deformation and regeneration of the hydrogel was evaluated by time-dependent thixotropicity, a hysteresis loop test, dynamic moduli, and creep-recovery measurements. In the time-dependent thixotropy (Fig. 3a), the first step in the low-shear condition achieved a stable η-value, which was used as a reference value for the viscosity-at-rest (*e.g.* gel loaded in a syringe). The second step, with higher shear rate, showed structural deformation (*e.g.* gel being injected through a needle), while the third step back to the low shear-rate showed structural regeneration (*e.g.* gel delivered into the host environment). As shown in Fig. 3a, the time-dependent thixotropy was significantly influenced by the concentration of the hydrogel. The percentage of regeneration was determined at the constant viscosity at step three, in relation to the reference value of the viscosity-at-rest. The regeneration percentages of the hydrogel were 58, 65, and 41% at concentrations of 1, 0.75, and 0.5%, respectively, whereas the total thixotropy times were 64, 97, and 98 s (Table S1). Interestingly, the presence of media significantly increased the regeneration of the hydrogel by ~71% at 0.75% concentration and ~78% at 0.5% concentration of the hydrogel (Fig. S5).

The hysteresis loop test is a classical method for the evaluation of thixotropic behavior. The relative percentage of the thixotropy area (A_r) of the CNF was inversely related to the concentration: 30.15, 37.10, and 46.29% at concentrations of 1, 0.75, and 0.5%, respectively (Fig. 3b; Table S1). The CNF hydrogel (1% w/w) was also analyzed for a subsequent continuous stress-ramp cycle (up to five cycles) to determine the structure recovery cycle performance and showed significant

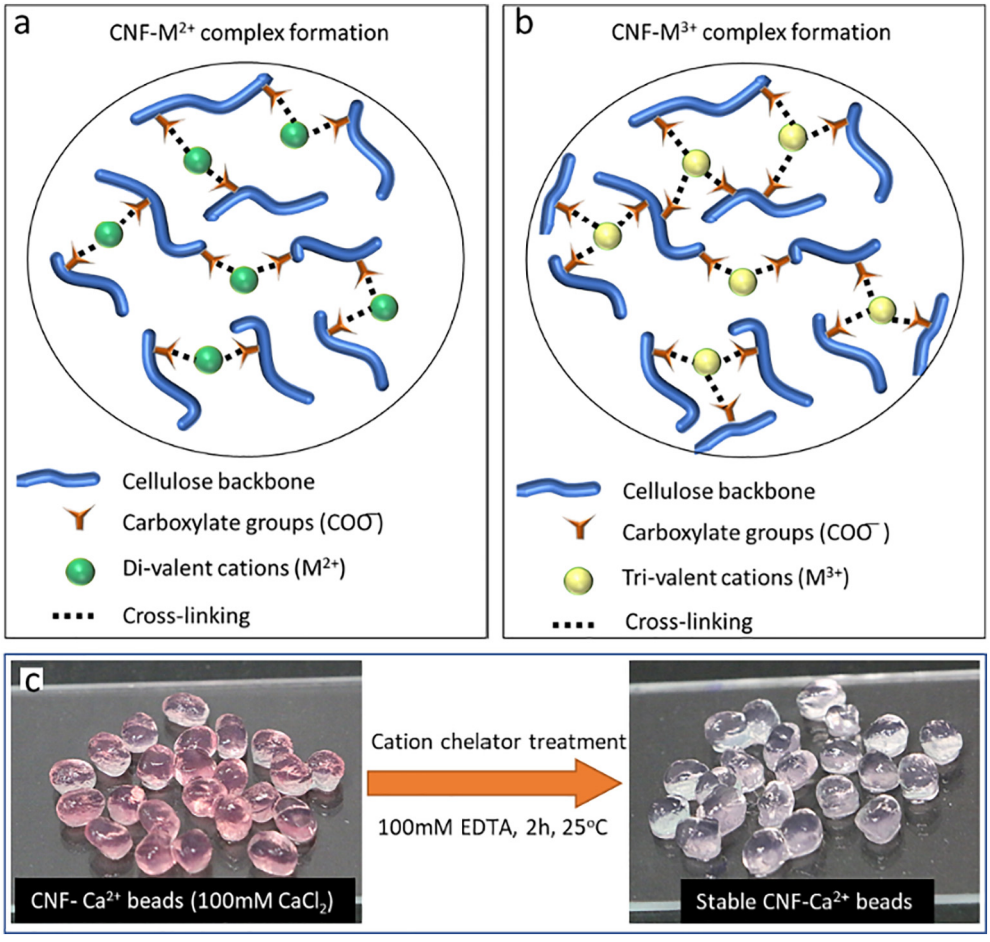

Fig. 5. Schematic illustration of CNF interfibrillar crosslinking with (a) di-valent (involving 2-chains) and (b) tri-valent (involving 3-chains) cations. (c) Stability test of the beads of the CNF-cation complex in the presence of a cationic chelator.

structure recovery even after five cycles (Fig. 3c). Additionally, the presence of media decreased the area of the hysteresis loop to 19.40% (0.75% with media) and 22.65% (0.5% with media) that of the control hydrogel (Fig. S6). Interestingly, the CNF hydrogel had significantly greater thixotropicity at low concentrations than sodium alginate (6.17% thixotropicity at 4% w/w concentration) [19]. The inverse trend of thixotropicity against concentration could be an advantage for injectable applications, where material density/viscosity *versus* thixotropy could form a tailored application system.

A frequency sweep test was performed to determine the storage (G′) and loss (G″) moduli as a function of angular frequency (ω) at the oscillation strain of the LVR region. The frequency sweep curves show that G′ varied from ~36 to 301 Pa as the concentration increased from 0.5 to 1% (Fig. S7). The structured gel showed elastic behavior ($G' \approx \omega^0$, $G' \gg G''$) [35] while the storage modulus (G′) was greater than the loss modulus (G″) at all three concentrations, representing a gel-like structure even at a high angular frequency (100 rad s^{-1}). Interestingly, these values are significantly higher than the hydrogel obtained from microcrystalline cellulose without surface oxidation, due to the stable structure formation on electrostatic repulsion between the polyanionic structure of the TEMPO-oxidized nanofibrils. To explore the recovery of the storage moduli (G′) of the gel upon relaxation, the CNF gel was deformed by applying high strain followed by relaxation (Fig. S8). The CNF gel showed significant structure recovery in terms of storage modulus (91.11%) even after 6 consecutive cycles of deformation-regeneration.

The CNF hydrogel exhibited structural fluid, non-Newtonian properties, thereby showing yield behavior. Yield stress (τ0) provides information about the relative strength of the network structure of the hydrogel; beyond the yield-stress value, the structure becomes compromised, and the material starts flowing. The yield stress of the CNF at concentrations of 1, 0.75, and 0.5% were 55.88, 23.08, and 6.89 Pa, respectively (Fig. S9a). The transient behavior of the viscoelastic property in the hydrogel samples was analyzed using creep-recovery tests at two shear stress steps (Fig. S9b). The first step was instantaneous stress applied for 300 s, with the strain increasing over time, known as creep. In the second step, the recovery was measured by removing the applied stress, with the strain decreasing over time. The maximum creep (peak strain) and the relative recovery were calculated from the creep-recovery plot (Table 1). The peak strain value of the CNF hydrogel at 0.5% concentration ($\gamma = 190.81\%$) was ~six-fold greater than for 1% CNF hydrogel ($\gamma = 33.14\%$) (Fig. S9; Table 1). On the other hand, the relative recovery of 0.5% hydrogel was 69.13%, compared to 18.94% at the higher concentration of CNF hydrogel (1%).

The results indicated higher peak strain associated with softer microstructures, which is good corroboration of the flow ramp curves discussed in Section 3.2. Interestingly, lower concentrations of CNF exhibited higher relative recovery, indicating greater elasticity in the microstructure, and the higher relative recovery indicated elasticity in the microstructures. The structure–property relationship and the diversity of the elasticity *versus* shear-thinning/thixotropicity behavior could enable a wide range of customized applications for the hydrogel.

3.4. Evaluation of stimulus responsiveness of CNF thixogel

The stimulus-responsive characteristics for the physical stimuli (shearing and sonication) and chemical stimuli (pH changes and cationic complexation) were confirmed by determining the storage modulus of the hydrogel (Figs. 4 & S10). The oscillation time sweep graph showed linear G′ (~100 Pa at 100 s) at rest. In the second step, G′ was measured immediately after the applied stimuli (shaking and sonication) and exhibited a significant decrease in storage modulus (28.37 and 60.82 Pa, respectively), which represented the hydrogel in a flowable state (Fig. 4b). On the removal of the external stimuli, the storage modulus of the hydrogel returned nearly to its previous condition due to the reversible structure formation. The shear-thinning and structure regenerative properties of the hydrogel enabled its injectable application and conformation to complex structures and narrow spaces (Fig. 4c & d). In the acidic pH (4.0), the hydrogel exhibited greater G′ (817.01 Pa) due to the protonation of the carboxylate groups. On the

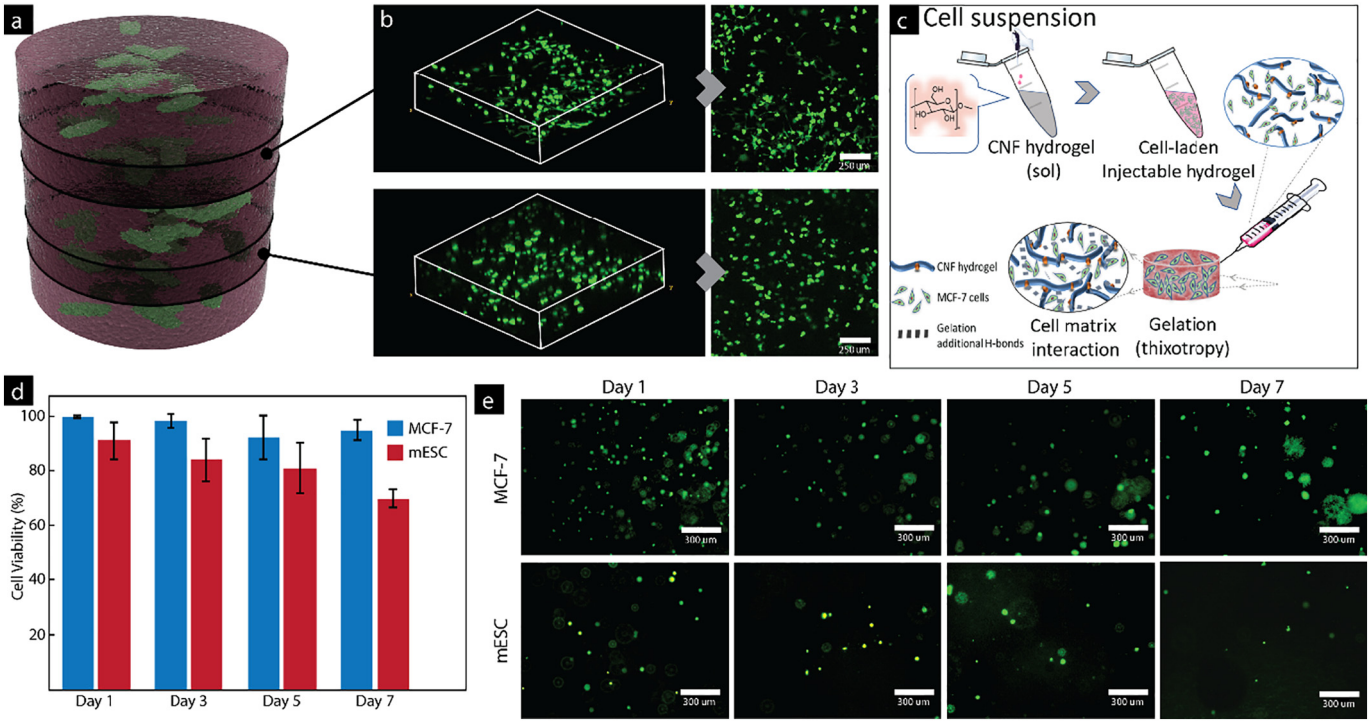

Fig. 6. CNF as a cell-encapsulation system. (a) Graphical representation of a cell-hydrogel construct and the areas of the hydrogel that were imaged using confocal microscopy. (b) Confocal microscopy images of GFP expressing MCF-7 cells cultured in cellulose hydrogels for 96 h. The left column presents 3D reconstructions of 600 μm thick confocal views of an 8 mm diameter cell-laden pillar; the right column presents the corresponding Z-axis maximum projection views. Scale bar: 250 μm. (c) Schematic illustration of a cell-delivery mechanism using the shear-thinning and thixotropy of CNF hydrogel. (d) Quantification of cell viability for MCF-7 and mESC cell lines. (e) Cell distribution in the thixogel during 1 week of culture.

other hand, the G′ value decreased sharply (27.84 Pa) in a base pH due to the lower cation–cation repulsion [36].

The responsive behavior of the TEMPO-oxidized cellulose hydrogel to applied stimuli, such as stress, sonication, or pH, enabled transit of the flowable solution and return to the hydrogel state upon removal of the external stimuli, demonstrating reversible flow behavior through several cycles. The substitution of the DI water phase of the hydrogel by DMEM maintained the switchable behavior of the system in response to external stimuli, enabling its use in combination with cell-culture techniques and demonstrating the suitability of the hydrogel for cell-encapsulation and cell-delivery systems (Fig. 4a).

The polyanionic cellulose also exhibited complex formation with di- and tri-valent cations ($M^{2+/3+}$), as previously reported [17,24]. The G′ was significantly greater with tri-valent (Fe^{3+}) ions (~17,972 Pa) than di-valent (Ca^{2+}) ions (1655.86 Pa) when interacting with three carboxyl groups from different glucuronan units at the same time, facilitating 3D bonding structures that yielded a more complex gel network (Fig. 5a & b) [37]. The ionic crosslinking ability of the hydrogel enabled formation of beads or filaments in the presence of the ionic solutions (*e.g.* 0.1% $CaCl_2$) (Fig. 5c; Movie S2). The cationic complex of the CNF was particularly stable and unaffected by the cationic chelator (EDTA), while obvious degradation has been reported with crosslinking complexes of other biopolymers (Fig. 5c) [38]. Additionally, CNF hydrogel dispersed in the DMEM exhibited slender water holding capacity (<10%) in the physiological pH condition (Fig. S11). Under acidic pH (4.0), most of the carboxylate anions were protonated, eliminating the main anion–anion repulsive forces, and consequently the water holding capacity decreased. At higher pH (~9), the charge-screening effect, due to the excess cations, shielded the —COO groups, preventing the anion–anion repulsion and leading to water loss from the structure.

3.5. Cell encapsulation and viability of CNF thixogel

The evaluation of CNF for cell encapsulation was studied for human breast cancer cells (MCF-7) and mESCs as models for sustained release of paracrine factors and for tissue regeneration, respectively. Due to the suitability of the material for showing liquid-like behavior after stimulation, the cells were easily encapsulated by shaking the cell-hydrogel mixture, resulting in a homogenous distribution that was retained when the hydrogel solidified (Fig. 6a & b). For breast cancer cells, the live cells that were identified as Calcein-positive and EthD-negative were constant at each time point for 1 week, with a 96% survival of cell population after 7 days post-encapsulation. In contrast, stem cells showed a significant decrease, of 18%, from the original population after a week of culture (Fig. 6c).

A similar, but larger (about 30%), decrease in embryonic stem cell populations, after 5 days of being encapsulated in alginate, hyaluronic acid, and Matrigel, has previously been reported [39]. This sudden population decrease, which resulted in a stable population at about day 10, is usually explained as the result of an increased hydrogel density by thermal gelation in the incubator [40]. That, however, does not explain why a similar effect is not observed in the cancerous line nor the independence of this effect from the encapsulating material.

For the two cell types investigated, a spherical, non-adherent morphology was observed (Fig. 6d). The spherical shape of the encapsulated cells in the 3D gel suggests that the cells were trapped within the hydrogel and not adhered to the cellulosic molecular chains. The lack of attachment also resulted in the inhibition of cellular aggregation—a common issue in cell-laden hydrogels [41,42] and the main limitation for the long-term survival of large tissue constructs, which fail due to the necrosis of the inner volumes of aggregates [43,44]. Therefore, the cellulose thixogel presented here may have potential as a vehicle for cell encapsulation and delivery, improving on the most common weaknesses of existing encapsulation materials, such as high cell mortality during delivery and necrosis of the cell-laden gel after implantation.

4. Conclusion

Here, we evaluated and examined the complete, comprehensive flow-deformation behavior of the oxidized CNF hydrogel. The material's properties were influenced by its concentration and the presence of external physical (*e.g.* stress, sonication) and chemical (*e.g.* pH and cations) stimuli or cell-culture media. The CNF hydrogel can be injected and exhibited characteristic shear-thinning behavior at a shear rate range of ~10 s^{-1}. Upon introduction, the hydrogel showed a rapid transformation from fluid to a structured hydrogel, achieving 58% regeneration in 60 s at 1% concentration. The CNF hydrogel formed 3D structures by flexible entanglement of nanofibers with a wide range of tunable moduli in G′ (~36–1000 Pa) based on concentration and in the presence of media. The soft and flexible hydrogel microstructure was confirmed by yield-stress behavior and high peak strain value (69.13%), even at low concentration (0.5%), in the creep-recovery study. The CNF hydrogel was highly compatible with the human breast cancer cells (MCF-7) and mESCs, with homogeneous distribution in the gel matrix, signifying its potential applicability as a cell-encapsulation delivery carrier for sustained release of paracrine factors and for tissue regeneration, with unique versatility for injection, scaffolding, and 3D bioprinting.

Additional data, including rheology plots, schematics, and additional discussion, are furnished in the online supporting information. Supplementary data to this article can be found online at https://doi.org/10.1016/j.ijbiomac.2019.02.135.

Conflicts of interest

There are no conflicts to declare.

Acknowledgments

This work was supported by the International Design Center (IDC) at the Singapore University of Technology and Design, the SUTD Digital Manufacturing and Design Centre (DManD), and the National Additive Manufacturing Innovation Cluster (NAMIC). The authors would like to thank Mr. Mak Kah Jun (MBI) for assistance during the confocal microscopy. Sincere thanks are also accorded to Dr. N Ray Dunn (IMB, ASTAR Singapore) for kindly providing the E14G2A cell line.

References

[1] J. Kopeček, Hydrogel biomaterials: a smart future? Biomaterials 28 (34) (2007) 5185–5192.
[2] J.L. Drury, D.J. Mooney, Hydrogels for tissue engineering: scaffold design variables and applications, Biomaterials 24 (24) (2003) 4337–4351.
[3] A. Chenite, C. Chaput, D. Wang, C. Combes, M.D. Buschmann, C.D. Hoemann, J.C. Leroux, B.L. Atkinson, F. Binette, A. Selmani, Novel injectable neutral solutions of chitosan form biodegradable gels in situ, Biomaterials 21 (21) (2000) 2155–2161.
[4] J.G. Fernandez, S. Seetharam, C. Ding, J. Feliz, E. Doherty, D.E. Ingber, Direct bonding of chitosan biomaterials to tissues using transglutaminase for surgical repair or device implantation, Tissue Eng. A 23 (3–4) (2017) 135–142.
[5] P. Moshayedi, G. Ng, J.C.F. Kwok, G.S.H. Yeo, C.E. Bryant, J.W. Fawcett, K. Franze, J. Guck, The relationship between glial cell mechanosensitivity and foreign body reactions in the central nervous system, Biomaterials 35 (13) (2014) 3919–3925.
[6] T.R. Hoare, D.S. Kohane, Hydrogels in drug delivery: progress and challenges, Polymer 49 (8) (2008) 1993–2007.
[7] C.L. Salgado, E.M.S. Sanchez, C.A.C. Zavaglia, A.B. Almeida, P.L. Granja, Injectable biodegradable polycaprolactone–sebacic acid gels for bone tissue engineering, Tissue Eng. A 18 (1–2) (2012) 137–146.
[8] M.B. Evangelista, S.X. Hsiong, R. Fernandes, P. Sampaio, H.-J. Kong, C.C. Barrias, R. Salema, M.A. Barbosa, D.J. Mooney, P.L. Granja, Upregulation of bone cell differentiation through immobilization within a synthetic extracellular matrix, Biomaterials 28 (25) (2007) 3644–3655.
[9] K.B. Fonseca, S.J. Bidarra, M.J. Oliveira, P.L. Granja, C.C. Barrias, Molecularly designed alginate hydrogels susceptible to local proteolysis as three-dimensional cellular microenvironments, Acta Biomater. 7 (4) (2011) 1674–1682.
[10] S.J. Bidarra, C.C. Barrias, M.A. Barbosa, R. Soares, P.L. Granja, Immobilization of human mesenchymal stem cells within RGD-grafted alginate microspheres and assessment of their angiogenic potential, Biomacromolecules 11 (8) (2010) 1956–1964.

[11] F. Munarin, S.G. Guerreiro, M.A. Grellier, M.C. Tanzi, M.A. Barbosa, P. Petrini, P.L. Granja, Pectin-based injectable biomaterials for bone tissue engineering, Biomacromolecules 12 (3) (2011) 568–577.
[12] R.G. Payne, M.J. Yaszemski, A.W. Yasko, A.G. Mikos, Development of an injectable, in situ crosslinkable, degradable polymeric carrier for osteogenic cell populations. Part 1. Encapsulation of marrow stromal osteoblasts in surface crosslinked gelatin microparticles, Biomaterials 23 (22) (2002) 4359–4371.
[13] M.-C. Li, Q. Wu, K. Song, Y. Qing, Y. Wu, Cellulose nanoparticles as modifiers for rheology and fluid loss in bentonite water-based fluids, ACS Appl. Mater. Interfaces 7 (8) (2015) 5006–5016.
[14] Y. Cheng, X. Luo, G.F. Payne, G.W. Rubloff, Biofabrication: programmable assembly of polysaccharide hydrogels in microfluidics as biocompatible scaffolds, J. Mater. Chem. 22 (16) (2012) 7659–7666.
[15] N.D. Sanandiya, A.K. Siddhanta, Cellulose-based spreadable new thixo gels: synthesis and their characterization, RSC Adv. 6 (95) (2016) 92953–92961.
[16] D.R. Chejara, M. Mabrouk, R.V. Badhe, J.A.S. Mulla, P. Kumar, Y.E. Choonara, L.C. du Toit, V. Pillay, A bio-injectable algin-aminocaproic acid thixogel with tri-stimuli responsiveness, Carbohydr. Polym. 135 (2016) 324–333.
[17] A.D. Dwivedi, N.D. Sanandiya, J.P. Singh, S.M. Husnain, K.H. Chae, D.S. Hwang, Y.-S. Chang, Tuning and characterizing nanocellulose interface for enhanced removal of dual-sorbate (AsV and CrVI) from water matrices, ACS Sustain. Chem. Eng. 5 (1) (2017) 518–528.
[18] H.-L. Nguyen, Y. Jo, M. Cha, Y. Cha, D. Yoon, N. Sanandiya, E. Prajatelistia, D. Oh, D. Hwang, Mussel-inspired anisotropic nanocellulose and silver nanoparticle composite with improved mechanical properties, electrical conductivity and antibacterial activity, Polymers 8 (3) (2016) 102.
[19] D.R. Chejara, S. Kondaveeti, K. Prasad, A.K. Siddhanta, Studies on the structure-property relationship of sodium alginate based thixotropic hydrogels, RSC Adv. 3 (36) (2013) 15744–15751.
[20] J. Yang, S. Chen, Y. Fang, Viscosity study of interactions between sodium alginate and CTAB in dilute solutions at different pH values, Carbohydr. Polym. 75 (2) (2009) 333–337.
[21] A.K. Siddhanta, N.D. Sanandiya, D.R. Chejara, S. Kondaveeti, Functional modification mediated value addition of seaweed polysaccharides – a perspective, RSC Adv. 5 (73) (2015) 59226–59239.
[22] X. Xu, F. Liu, L. Jiang, J.Y. Zhu, D. Haagenson, D.P. Wiesenborn, Cellulose nanocrystals vs. cellulose nanofibrils: a comparative study on their microstructures and effects as polymer reinforcing agents, ACS Appl. Mater. Interfaces 5 (8) (2013) 2999–3009.
[23] T. Saito, S. Kimura, Y. Nishiyama, A. Isogai, Cellulose nanofibers prepared by TEMPO-mediated oxidation of native cellulose, Biomacromolecules 8 (8) (2007) 2485–2491.
[24] N.D. Sanandiya, A.K. Siddhanta, Facile synthesis of a new fluorogenic metal scavenging interpolymeric diamide based on cellulose and alginic acids, Carbohydr. Res. 381 (2013) 93–100.
[25] L. Segal, J.J. Creely, A.E. Martin Jr., C.M. Conrad, An empirical method for estimating the degree of crystallinity of native cellulose using the X-ray diffractometer, Text. Res. J. 29 (10) (1959) 786–794.
[26] D. da Silva Perez, S. Montanari, M.R. Vignon, TEMPO-mediated oxidation of cellulose III, Biomacromolecules 4 (5) (2003) 1417–1425.
[27] M. Dolz, F. González, J. Delegido, M.J. Hernández, J. Pellicer, A time-dependent expression for thixotropic areas. Application to Aerosil 200 hydrogels, J. Pharm. Sci. 89 (6) (2000) 790–797.
[28] M. Sharma, D. Mondal, C. Mukesh, K. Prasad, Preparation of tamarind gum based soft ion gels having thixotropic properties, Carbohydr. Polym. 102 (2014) 467–471.
[29] N.D. Sanandiya, Y. Vijay, M. Dimopoulou, S. Dritsas, J.G. Fernandez, Large-scale additive manufacturing with bioinspired cellulosic materials, Sci. Rep. 8 (1) (2018) 8642.
[30] C. Loebel, C.B. Rodell, M.H. Chen, J.A. Burdick, Shear-thinning and self-healing hydrogels as injectable therapeutics and for 3D-printing, Nat. Protoc. 12 (8) (2017) 1521–1541.
[31] J. Venkatesan, D.S. Sankar, K. Hemalatha, Y. Yatim, Mathematical analysis of Casson fluid model for blood rheology in stenosed narrow arteries, J. Appl. Math. 2013 (2013) 11.
[32] T.G. Mezger, The Rheology Handbook: For Users of Rotational and Oscillatory Rheometers, 2nd ed., Vincentz Network GmbH & Co KG2006.
[33] M.-C. Li, Q. Wu, K. Song, S. Lee, Y. Qing, Y. Wu, Cellulose nanoparticles: structure–morphology–rheology relationships, ACS Sustain. Chem. Eng. 3 (5) (2015) 821–832.
[34] N. Russ, B.I. Zielbauer, T.A. Vilgis, Impact of sucrose and trehalose on different agarose-hydrocolloid systems, Food Hydrocoll. 41 (2014) 44–52.
[35] G.M. Kavanagh, S.B. Ross-Murphy, Rheological characterisation of polymer gels, Prog. Polym. Sci. 23 (3) (1998) 533–562.
[36] Ali Pourjavadi, S. Barzegar, Synthesis and evaluation of pH and thermosensitive pectin-based superabsorbent hydrogel for oral drug delivery systems, Starch - Stärke 61 (3–4) (2009) 161–172.
[37] C.H. Yang, M.X. Wang, H. Haider, J.H. Yang, J.-Y. Sun, Y.M. Chen, J. Zhou, Z. Suo, Strengthening alginate/polyacrylamide hydrogels using various multivalent cations, ACS Appl. Mater. Interfaces 5 (21) (2013) 10418–10422.
[38] U. Schlemmer, Studies of the binding of copper, zinc and calcium to pectin, alginate, carrageenan and gum guar in HCO−3·CO2 buffer, Food Chem. 32 (3) (1989) 223–234.
[39] G. Marchioli, L. van Gurp, P.P. van Krieken, D. Stamatialis, M. Engelse, C.A. van Blitterswijk, M.B. Karperien, E. de Koning, J. Alblas, L. Moroni, A.A. van Apeldoorn, Fabrication of three-dimensional bioplotted hydrogel scaffolds for islets of Langerhans transplantation, Biofabrication 7 (2) (2015), 025009. .
[40] W. Hassan, Y. Dong, W. Wang, Encapsulation and 3D culture of human adipose-derived stem cells in an in-situ crosslinked hybrid hydrogel composed of PEG-based hyperbranched copolymer and hyaluronic acid, Stem Cell Res Ther 4 (2) (2013) 32.
[41] H.J. Klassen, T.F. Ng, Y. Kurimoto, I. Kirov, M. Shatos, P. Coffey, M.J. Young, Multipotent retinal progenitors express developmental markers, differentiate into retinal neurons, and preserve light-mediated behavior, Invest. Ophthalmol. Vis. Sci. 45 (11) (2004) 4167–4173.
[42] S.-F. Lan, B. Safiejko-Mroczka, B. Starly, Long-term cultivation of HepG2 liver cells encapsulated in alginate hydrogels: a study of cell viability, morphology and drug metabolism, Toxicol. in Vitro 24 (4) (2010) 1314–1323.
[43] V.L. Tsang, A.A. Chen, L.M. Cho, K.D. Jadin, R.L. Sah, S. DeLong, J.L. West, S.N. Bhatia, Fabrication of 3D hepatic tissues by additive photopatterning of cellular hydrogels, FASEB J. 21 (3) (2007) 790–801.
[44] J.G. Fernandez, A. Khademhosseini, Micro-masonry: construction of 3D structures by microscale self-assembly, Adv. Mater. 22 (23) (2010) 2538–2541.